Biosensors and Bioelectronics 49 (2013) 466–471

Contents lists available at SciVerse ScienceDirect

Biosensors and Bioelectronics

journal homepage: www.elsevier.com/locate/bios

Bioinspired polydopamine as the scaffold for the active AuNPs anchoring and the chemical simultaneously reduced graphene oxide: Characterization and the enhanced biosensing application

Juan Tian [a,b], Sheng-Yuan Deng [a], Da-Li Li [a], Dan Shan [a,b,*], Wei He [a], Xue-Ji Zhang [a,*], You Shi [a]

[a] School of Environmental and Biological Engineering, Nanjing University of Science and Technology, Nanjing 210094, China
[b] School of Chemistry & Chemical Engineering, Yangzhou University, Yangzhou 225002, China

ARTICLE INFO

Article history:
Received 17 April 2013
Received in revised form
30 May 2013
Accepted 5 June 2013
Available online 13 June 2013

Keywords:
Graphene oxide
Surface functionalization
Polydopamine
NADH
Alcohol dehydrogenase
AuNPs

ABSTRACT

We report here an efficient approach to enhance the performance of biosensing platform based on graphene or graphene derivate. Initially, graphene oxides (GO) nanosheets were reduced and surface functionalized by one-step oxidative polymerization of dopamine in basic solution at environment friendly condition to obtain the polydopamine (Pdop) modified reduced graphene oxides (PDRGO). The bioinspired surface was further used as a support to anchor active gold nanoparticles (AuNPs). The morphology and structure of the as-prepared AuNPs/PDRGO nanocomposite were investigated by field-emission scanning electron microscopy (FESEM), transmission electron microscopy (TEM), Fourier transform-infrared spectroscopy (FT-IR). Electrochemical studies demonstrate that the as-prepared AuNPs/PDRGO hybrid materials possess excellent electrochemical properties and electrocatalytic activity toward the oxidation of NADH at low potential (0.1 V vs. SCE) with the fast response (15 s) and the broad linear range (5.0×10^{-8}–4.2×10^{-5} M). Thus, this AuNPs/PDRGO nanocomposite can be further used to fabricate a sensitive alcohol biosensor using alcohol dehydrogenase (ADH), by simply incorporating the specific enzyme within the composite matrix with the aid of chitosan (Chit).

© 2013 Elsevier B.V. All rights reserved.

1. Introduction

Graphene has been considered as a “rising-star” material and received widespread attention due to its unique structure and outstanding physical properties (Geim and Novoselov, 2007; Novoselov et al., 2004). Because graphene sheets tend to form irreversible agglomerates or even restack to graphite through strong π–π stacking and van der Waals interaction, it is difficult for graphene to be directly dispersed into solvents to form a uniform dispersion (Li et al., 2009), which further limits its potential application in the construction of electrochemical sensing platforms. The chemical precursor of graphene, graphene oxide (GO), is basically a single atomic layer of carbon covered with epoxy, hydroxyl, carbonyl, and carboxyl groups (Compton and Nguyen, 2010; Chen et al., 2012). While these functional groups enable the suspension of GO in aqueous solution, their sp^2 network is partially destroyed. As a consequence, the conductivity of the GO is inferior to that of graphene. Therefore, many efforts have been devoted into graphene/GO modification to meet the desire of the enhanced performance-biosensing system (Kuila et al., 2011).

Most recently, Lee et al. introduced a distinctive approach to surface modification in which self-polymerization of dopamine produced an adherent polydopamine (Pdop) coating on a wide variety of materials by simple dip-coating with dopamine solution (Lee et al., 2007). Moreover, the formation of biocompatible “Pdop” thin films becomes a popular method to confer multifunctionality to solid–liquid interfaces through the available catechol groups of such films (Lee et al., 2007).

Encouraged by the advantageous properties of the Pdop, in this work, we developed a simple and efficient route for constructing an enhanced performance-biosensing platform based on AuNPs/PDRGO hybrid system of simple ingredients. GO nanosheets was readily reduced by dopamine and chemical functionalization allows the graphene nanosheets to disperse more easily in aqueous solution. Due to the catechol moiety present in Pdop coating, active Au particles were anchored subsequently by “electroless metallization”. Additionally, the Pdop is coated onto a properly RGO sheet, it may exhibit high electrical conductivity because of π–π stacking (Yang et al., 2012). The residual catechol moiety of

* Corresponding authors at: School of Environmental and Biological Engineering, Nanjing University of Science and Technology, Nanjing 210094, China. Tel./fax: +0086 25 84303107.
E-mail addresses: danshan@njust.edu.cn, danshan@yzu.edu.cn (D. Shan), drxuejizhang@gmail.com (X.-J. Zhang).

0956-5663/$ - see front matter © 2013 Elsevier B.V. All rights reserved.
http://dx.doi.org/10.1016/j.bios.2013.06.009

AuNPs/PDRGO hybrid system may allow for further turning of the redox potential of the quinone/hydroquinone couple toward NADH oxidation at lower overpotential (Maleki et al., 2012).

2. Experimental section

2.1. Materials

Alcohol dehydrogenase (ADH) (EC 1.1.1.1, from *Saccharomyces cerecisiae*, ≥300 units mg^{-1}), β-nicotinamide adenine dinucleotide reduced disodium salt hydrate (NADH) and β-nicotinamide adenine dinucleotide sodium salt from *Saccharomyces cerevisiae* (NAD^+) were purchased from Sigma. Graphene oxide (GO) was made from graphite flake nature foreign. Dopamine hydrochloride was from Aladin. $HAuCl_4 \cdot 4H_2O$ was obtained from Shanghai Chemical Reagent (Shanghai, China). Tris(hydroxymethyl)aminomethane hydrochloride (Tris) and chitosan (Chit, M_W: ~1×10^6; > 90%, deacetylation) were purchased from Sinopharm Chemical Reagent Co., Ltd. All other chemicals were of analytical grade and used without further purification. Phosphate buffer solution (PBS) was 0.1 M K_2HPO_4 and KH_2PO_4 and its pH was adjusted with H_3PO_4 or KOH solutions. Double-distilled water was used throughout the experiment.

2.2. Measurements and apparatus

UV–vis measurements were conducted by using Shimadzu UV-3600 PC UV–visible spectrometer. Fourier transform infrared (FT-IR) spectra of the samples were measured on a Prestige-21spectrometer. Field-emission scanning electron microscopy (FESEM) was carried out with a XL-30E scanning electron microscope operated at an accelerating voltage of 15 kV. Transmission electron microscopy (TEM) and high resolution transmission electron microscopy (HRTEM) were performed on a Philips TECNAI-12 instrument.

A CHI 760D electrochemical workstation (CH Instrument) was used for cyclic and amperometric voltammetry. A three-electrode cell was used with a saturated calomel electrode (SCE) as reference electrode, a platinum wire as counter electrode, and the modified GCE (diameter 3 mm) as working electrode polished carefully with 0.05 μm alumina particles on silk followed by rinsing with the distilled water and dried in air before use.

2.3. Synthesis of PDRGO and AuNPs/PDRGO nanocomposites

The procedure of the synthesis of PDRGO and AuNPs/PDRGO nanocomposite is very straightforward as illustrated in Scheme 1. In the foremost step, GO was reduced and surface functionalized simultaneously by mixing an aqueous suspension of GO (1 mg mL^{-1}) with a solution of dopamine hydrochloride (1 mg mL^{-1}, 10 mM Tris buffer, pH 8.5). After magnetically stirring for 14 h at room temperature, the yellow brown GO suspension turned into a black solution. PDRGO was centrifuged and dispersed in distilled water for wash in turn 3 times. The products were collected, washed and dried under vacuum at 60 °C.

In the second step, the black PDRGO suspension (1.5 mg mL^{-1}) was prepared by dispersing the above-obtained PDRGO in deionized water under sonication. Prior to AuNPs loading, all glasswares were soaked in a mixture of nitric acid (45 mL) and hydrochloric acid (135 mL) for 1 h, and then thoroughly washed with deionized water. 1.2 mL $HAuCl_4 \cdot 4H_2O$ (10 mg mL^{-1}) aqueous solution was added to the above-prepared PDRGO suspension (20 mL), and the mixture was vigorously stirred and turned to erythrine. Two hours later, an aqueous solution of sodium borohydride (0.1 mol L^{-1}) was added and stirring continued for the other 2 h. In this chemical reduction process, both GO and Au ions are reduced completely. The final obtained products were collected, washed and dried under vacuum at 60 °C.

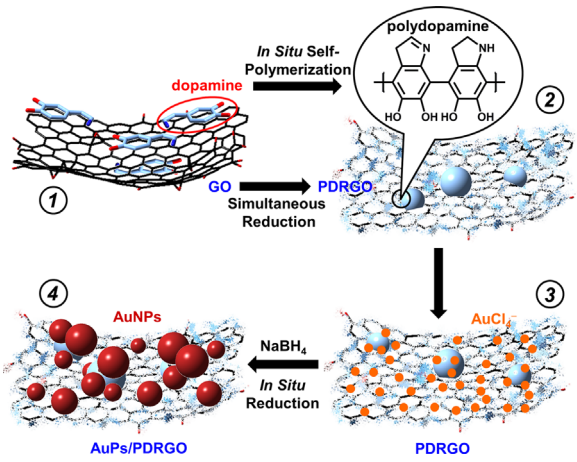

Scheme 1. Illustration of the synthesis of PDRGO and AuNPs/PDRGO nanocomposites.

2.4. Preparation of GO, PDRGO and AuNPs/PDRGO modified electrodes

GO/GCE, PDRGO/GCE and AuNPs/PDRGO were prepared following the same protocol described below: (1) the suspensions (1 mg mL^{-1}) of GO, PDRGO and AuNPs/PDRGO were prepared by dispersing the corresponding products in deionized water under ultrasonic and (2) 10 μL of the suspension was spread on the surface of bare GCE and dried in air.

2.5. Preparation of alcohol biosensor

In this work, Chit was used as enzyme immobilization matrix. To obtain good responses of alcohol biosensor, the following conditions were optimized in control experiments. A Chit solution (2 mg mL^{-1}) was prepared by dissolving Chit flakes in 1.0 wt% acetic acid (HAc). ADH and NAD^+ were dissolved in 0.1 M PBS (pH 7.5) with a concentration of 10 mg mL^{-1} and 1 M, respectively. The defined amount of aqueous ADH–NAD^+/Chit mixture was spread on the surface of as-prepared AuNPs/PDRGO/GCE. Before use, the enzyme electrode was rinsed under stirring for 20 min with buffer solution to remove the enzyme not firmly immobilized.

3. Results and discussion

3.1. Synthesis and structure characterization of AuNPs/Pdop/RGO nanocomposite

The electrochemical and catalytic behaviors of AuNPs/PDRGO highly depend on not only the property of the anchored AuNPs (i.e., size and dispersity), but also the formed Pdop film (i.e., thickness and the amount of superficial catechol groups) on the RGO surface. The superficial catechol groups play the important role in the reduction of Au^{3+} to Au^0, the stabilization of formed AuNPs and even the redox electrochemical reaction. The size and dispersity of AuNPs show strong dependence on the dosage of $HAuCl_4$. Thus, AuNPs/PDRGO nanocomposites described below are prepared under the optimal conditions by controlling the dosage of $HAuCl_4$ and dopamine and even the reaction time.

Fig. 1A shows UV–vis spectra of dopamine, Pdop, GO and PDRGO. The adsorption peak of the dopamine appears at 275 nm

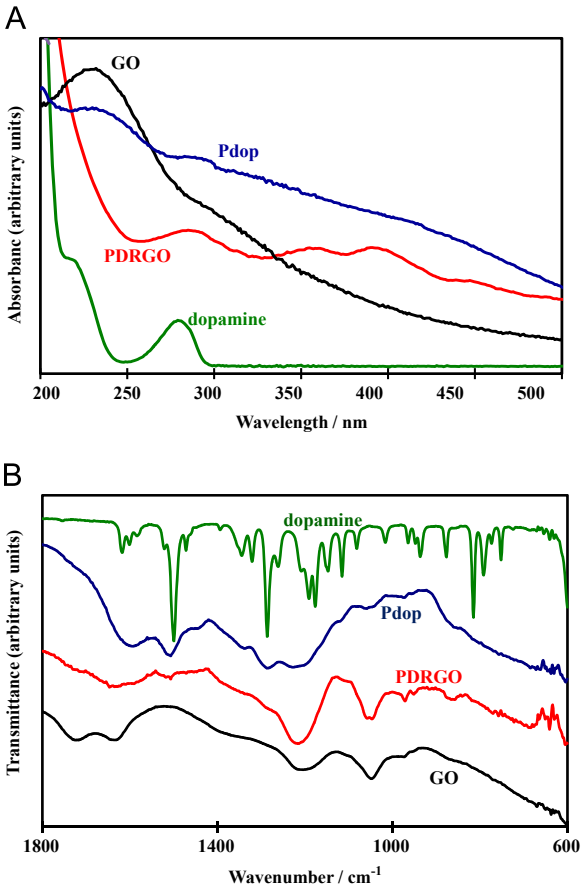

Fig. 1. UV–vis (A) and FTIR (B) spectra of dopamine, Pdop, GO and PDRGO.

(curve a of Fig. 1A), as reported in the literature (Feng et al., 2012). The peak almost disappears after the self-polymerization. Furthermore, there are two ultra-weak waves located at around 231 nm and 283 nm, which are originated from the π–π^* electron transition of the Pdop (curve b of Fig. 1A). Comparing the UV–vis spectra between GO (curve c of Fig. 1A) and PDRGO (curve d of Fig. 1A), 223 nm absorbance peak characteristic of GO disappeared and a new weak wave at around 285 nm was detected, which is a characteristic absorption of Pdop due to the presence of catechols (Liu et al., 2012). It indicates that GO is probably reduced and surface modified in one step by the release of electrons during the oxidative polymerization of dopamine–hydrochloride by oxygen in the air (Kang et al., 2011).

The simultaneous reduction and surface function of GO to Pdop modified RGO (PDRGO) was further confirmed by FT-IR illustrated in Fig.1B. As small molecule, FT-IT spectrum of dopamine displays many strong absorption peaks (curve a of Fig. 1B). In the spectrum of GO (curve c of Fig. 1B), the peaks at 1713 cm^{-1}, 1624 cm^{-1}, 1203 cm^{-1} and 1037 cm^{-1} were assigned to the stretching vibration of C=O bond, C=C of aromatic ring, C–O bond, and C–O–C respectively. FT-IR spectrum of PDRGO exhibits typical peaks for both Pdop and GO (curve d of Fig. 1B). The weak band at 1438 cm^{-1} corresponds to the C–C vibration of the benzene ring moiety. The peaks at 1499 cm^{-1} and 1211 cm^{-1} were assigned to the N–H shearing vibration of the amide group and phenolic C–OH stretching vibration, respectively, confirmed the polymerization of dopamine and presence of coated Pdop layer on RGO. The disappearance of the C=O peak at 1713 cm^{-1} compared to GO provided a solid demonstration of GO reduction. Strongly indicates that GO was reduced by one-step Pdop functionalization.

3.2. Morphology of the PDRGO and AuNPs/PDRGO nanocomposite

FESEM and TEM techniques were used to obtain direct visualization of PDRGO and AuNPs/PDRGO. Obviously, the surface morphology of the composite is much different from those of PDRGO and AuNPs/PDRGO as portrayed in Fig. 2. The surface of pure GO modified GCE is smooth with a few thin wrinkles (inset of Fig. 2A). After reduced and surface modification by dopamine, the morphology of DPRGO/GCE remains the inherent GO sheets of wrinkles with the relative think coating (Fig. 2A). As indicated in the magnified TEM image of DPRGO (Fig. 2C), the observation confirms further that GO nanosheet was wrapped uniformly by a coating of Pdop with small nanoparticles. In the oxidation of dopamine, Pdop layer is preferentially generated on the surface of the GO nanosheet. The small spherical nanoparticles of Pdop can be only formed at the condition of excess dopamine. As shown in Fig. 2B and D, a great amount of AuNPs with obvious agglomeration are observed on Pdop modified GO sheets. The Au^{3+} ions were first reduced to Au^0 by the superficial catechol groups and then the Au^0 species aggregated to AuNPs. Possibly due to the groups in the surface is limited, the stabilization interactions between the Pdop groups with AuNPs is somewhat weak, which leads to the growth of large-size AuNPs (Zeng et al., 2012). The further agglomeration may happen when the increased Au^{3+} were further reduced by $NaBH_4$. Energy-dispersive X-ray analysis (EDX, Fig. 2E) demonstrates that the chemical composition of AuNPs/PDRGO sample contains gold, oxygen, nitrogen, and carbon, indicating the successful loading of AuNPs on the PDRGO sheets. In order to provide more detailed structural information about the products, high resolution transmission electron microscopy was performed. The average diameter of AuNPs is around 12 nm (Inset of Fig. 2D). This conductive AuNPs/PDRGO may establish electrical conduction pathways throughout the whole composite, which is responsible for the electrical conductivity and electrochemical sensing.

3.3. Electrochemical response of AuNPs/PDRGO-modified electrode to NADH

The detection of NADH is of great importance because it is produced in reactions that are catalyzed by hundreds of dehydrogenases. In order to test the potential electrocatalytic activities of the AuNPs/PDRGO nanohybrids, cyclic voltammetric responses were recorded at those bare and modified electrodes in the absence and presence of NADH. As shown in Fig. 3, upon the addition of 1.0 mM NADH, the anodic peak currents increase accompanied by reduced cathodic peak currents in all cases. The NADH oxidation process emerges at a high positive potential over than 0.6 V at the bare GCE (Fig. 3A), as the previous report (Yang and Liu, 2009). The potential of NADH oxidation is lowered to 0.4 V using GO/GCE (Fig. 3B). This indicates that the graphene can decrease the overpotential of NADH oxidation at the surface of electrode and facilitate electrochemical oxidation of NADH. That might be related to the excellent property of graphene, such as high specific surface area and electrical conductivity. For the case of electrode modified by PDRGO/GCE, in 0.1 M PBS (pH 7.0), a wide oxidation wave ascribes to the electroactive signal of Pdop. Upon addition of NADH, the dramatic increase of oxidation current occurs at near 0.4 V. The maximum oxidation current is about 4.8-fold larger than that obtained by GO/GCE (Fig. 3C). It is well known that quinone functionalities can mediate electron transfer from NADH (Wu et al., 2007). Thus, the higher oxidation current may be due to the mediated electrocatalytic oxidation of NADH by catechol moiety present in Pdop. The further enhanced oxidation of NADH can be obtained by AuNPs/PDRGO/GCE as shown in Fig. 3D. The substantial negative shift with an onset potential at ca.

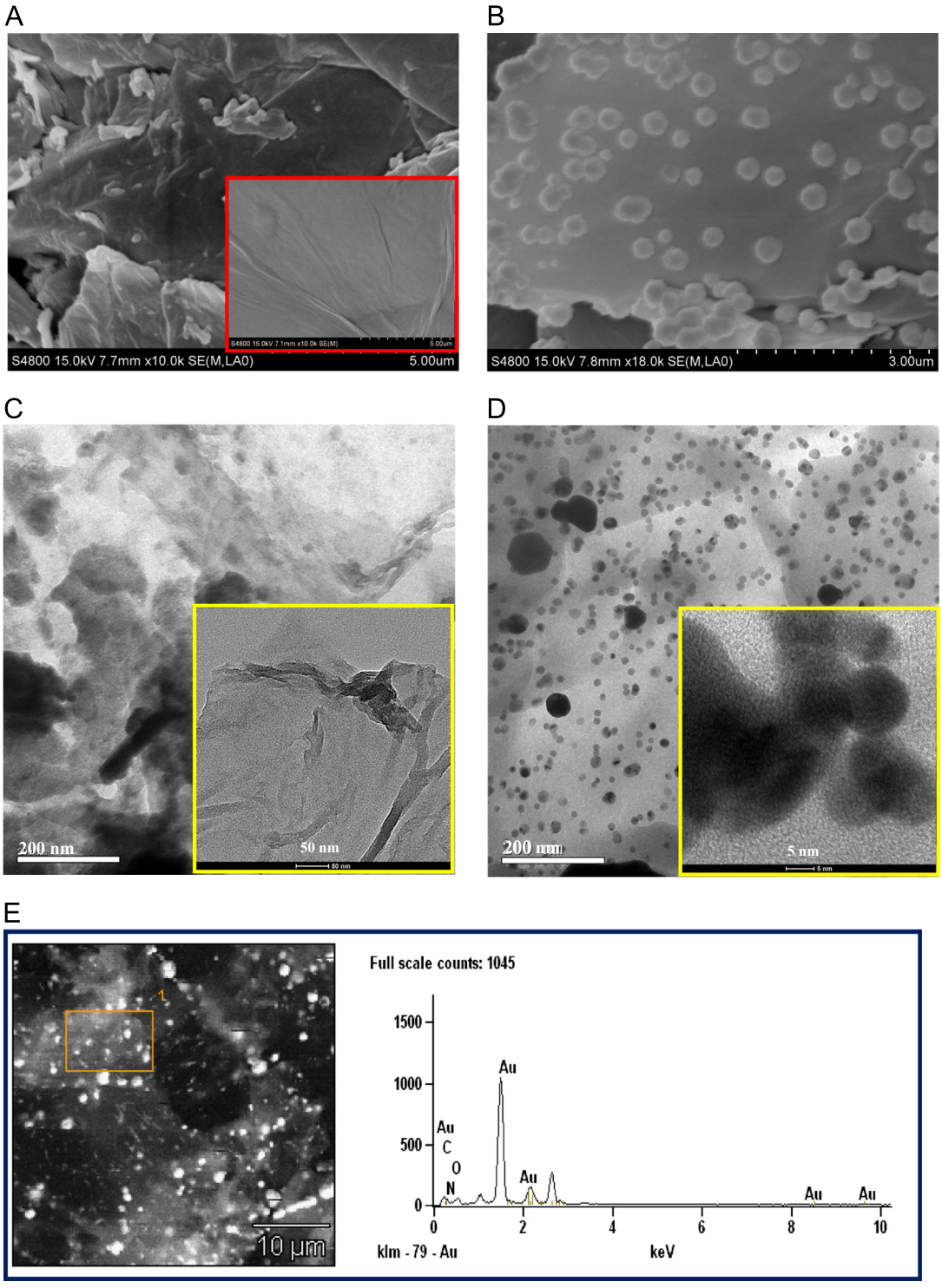

Fig. 2. (A) SEM image of the electrode surface modified by PDRGO (inset: SEM image of the electrode surface modified by pure GO); (B) SEM image of the electrode surface modified by AuNPs/PDRGO; (C) TEM and HRTEM (inset) images of PDRGO; (D) TEM and HRTEM (inset) images of AuNPs/PDRGO and (E) EDX pattern of AuNPs/PDRGO.

−0.23 V and 6.5-fold larger current signal demonstrate that AuNPs/PDRGO can facilitate the oxidation of NADH greatly.

The amperometric measurement of the AuNPs/PDA/GO/GCE to NADH at an applied potential of 0.1 V upon successive addition of NADH into stirring 0.1 M PBS (pH 7.0) was performed (See Fig. 1S in the Supplementary data). Upon the addition of an aliquot of NADH to the buffer solution, the oxidation current increases steeply to reach a stable value. The proposed modified electrode achieves 95% of the steady-state current within 15 s. The corresponding calibration curve was illustrated in inset B of Fig. 1S in the Supplementary data. The response to NADH is linear in the range from 5.0×10^{-8} to 4.2×10^{-5} M, and with a linear regression equation for $i(\mu A)=2.82$ [NADH] (mM)+0.0024, $R^2=0.9983$ ($n=25$). Five different electrodes of AuNPs/PDA/GO were tested independently for the amperometric response to NADH, providing a RSD value of 4.9%. This indicates, in particular, an efficient and reproducible immobilization process although the procedure employed was a nonautomatic one. The operational stability of the AuNPs/PDA/GO/GCE was also examined. A

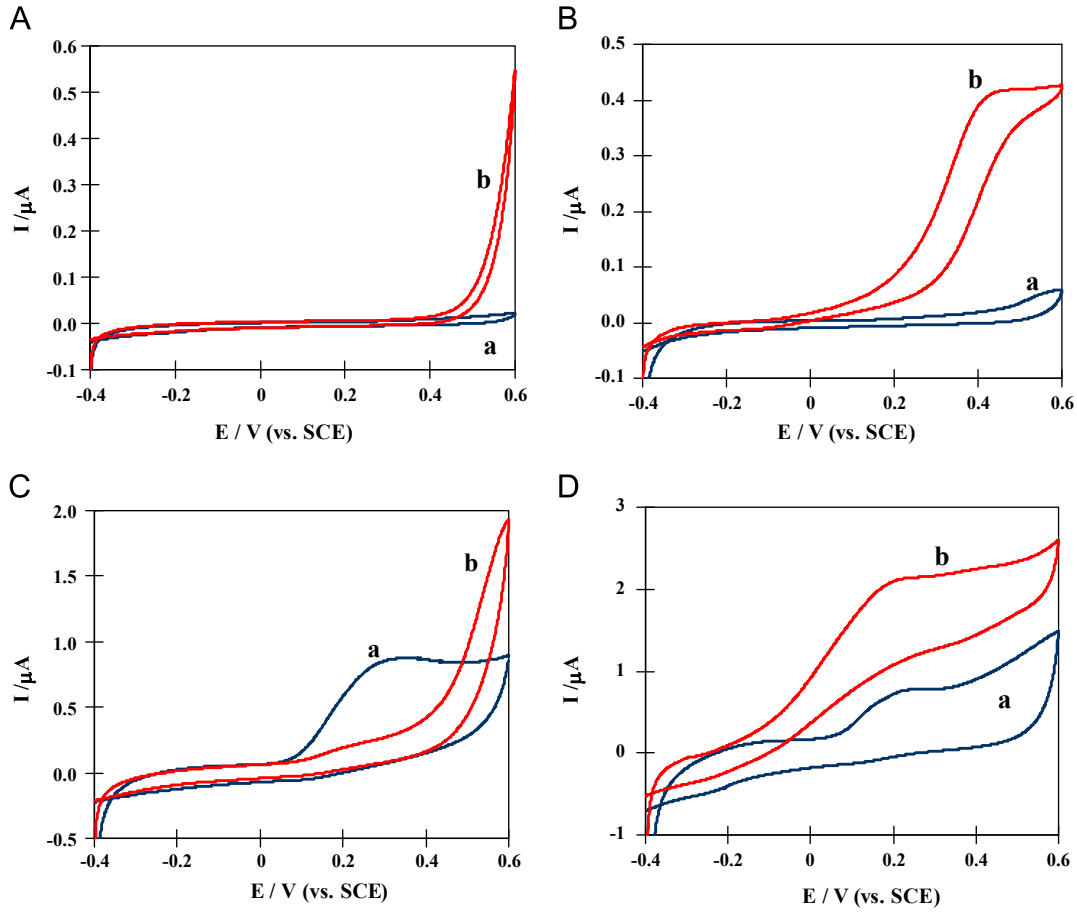

Fig. 3. Cyclic voltammograms of (A) bare GCE, (B) GO/GCE, (C) PDRGO/GCE and (D) AuNPs/PDRGO/GCE in N_2-saturated PBS (0.1 M, pH 7) in the absence (a) and presence of 1 mM NADH. Scan rate: 1 mV s^{-1}.

reproducible current response with a relative standard deviation (RSD) of 3.8% was observed in 25 successive assays of 1×10^{-6} M NADH.

3.4. Electroanalytical aspects of oxidation of ethanol

The excellent sensitivity and high precision of the proposed sensor towards the detection of NADH make it attractive for the further development of dehydrogenase-based electrochemical sensors. The dehydrogenase enzymes catalyze the oxidation of a variety of substrates in the presence of cofactor NAD^+, which can be applied in sensors and biotransformation design (Jena and Raj, 2006; Tang et al., 2009). Therefore, ADH was entrapped by AuNPs/PDRGO nanocomposite and the electrocatalytic activity of the ethanol biosensor was examined using cyclic voltammetry ranging from −0.2 to 0.4 V with the scan rate of 1 mV s^{-1} in 0.1 M PBS (pH 7.5) containing 5 mM NAD^+. In the presence of 2 mM ethanol, a distinguished catalytic effect is observed: an enhancement of the oxidation current and a concomitant decrease of the cathodic current (Inset A of Fig. 4).

Fig. 4 displays the amperometric response for successive addition of ethanol into a stirred 0.1 M PBS (pH 7.5) containing 5 mM NAD^+ recorded at the proposed biosensor under the operation potential of 0.3 V. Apparently, each addition of ethanol gives rise to a rise in current. The corresponding calibration curve is shown in inset B of Fig. 4. The linear response range of the biosensor was up to 3×10^{-3} M (R^2=0.994) with a detection limit of 8.8×10^{-5} M (S/N=3) and a sensitivity of 78.6 μA M cm^{-2}. Five different ethanol biosensors were tested independently for the amperometric response to ethanol, providing a RSD value of 7.8%.

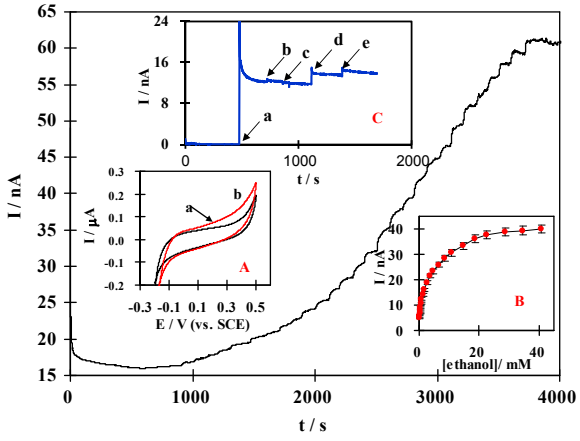

Fig. 4. Typical steady-state response of the alcohol biosensor on successive injection of alcohol into 10 ml of stirring 0.1 M PBS (pH 7.5) containing 5 mM NAD^+, applied potential: 0.3 V vs. SCE. **Inset A:** cyclic voltammograms of as-prepared alcohol sensor in 0.1 M PBS (pH 7.5) containing 5 mM NAD^+ in the absence (a) and presence of 2 mM ethanol (b) with the scan rate of 1 mV s^{-1}. **Inset B:** calibration curve of the proposed biosensor to ethanol. **Inset C:** steady-state current–time response of proposed alcohol biosensor to successive increments: (a) 2 mM ethanol; (b) 2 mM methanol; (c) 2 mM isopropanol; (d) 0.2 mM ascorbic acid and (e) 0.2 mM uric acid in a stirring 0.1 M PBS (pH 7.5) containing 5 mM NAD^+ with the applied potential of 0.3 V vs. SCE.

The stability of the proposed ethanol sensor stored at 4 °C was investigated by recording periodically its current response to 1×10^{-4} M ethanol. The response of the biosensor was unchanged during the initial three weeks. It still retained about 76% of its

original response after 52 days of storage. The effect of possible interfering species such as methanol, isopropanol, ascorbic acid and uric acid on ethanol detection has been examined (Inset of Fig. 4C). No appreciable signals were observed for the successive injection of the interferents into the electrolyte solution.

4. Conclusion

In summary, we have successfully constructed a novel bioelectrochemical sensing platform based on AuNPs/PDRGO nanocomposite. Assigning to the self-polymerization and reducibility of the dopamine, the reduction and surface functionalization of GO can be simultaneously achieved feasibly. The biocompatible Pdop self-adhered on the RGO remains the reductive nature and can work as both reductant and the protector of the metal nanoparticles. Moreover, the residue moiety of catechol in the AuNPs/PDRGO hybrid system can efficiently accelerate the electrochemical oxidation of NADH via electron transfer. This preliminary study provides a profound guidance to construct other enhanced electrochemical sensors.

Acknowledgments

This work was supported by the National Nature Sciences Foundation of China (Grant no. 21175114), the Natural Science Foundation of Jiangsu (BK2011441), Qing Lan Project of Jiangsu Province and NJUST Research Funding (Nos. 2011ZDJH17 and 2012ZDJH009), and the Fundamental Research Funds for the Central Universities (No. 30920130112012).

Appendix A. Supplementary information

Supplementary data associated with this article can be found in the online version at http://dx.doi.org/10.1016/j.bios.2013.06.009.

References

Chen, Q.W., Zhang, L.Y., Chen, G., 2012. Analytical Chemistry 84, 171–178.
Compton, O.C., Nguyen, S.T., 2010. Small 6, 711–723.
Feng, J.J., Zhang, P.P., Wang, A.J., Liao, Q.C., Xi, J.L., Chen, J.R., 2012. New Journal of Chemistry 36, 148–154.
Geim, A.K., Novoselov, K.S., 2007. Nature Materials 6, 183–191.
Jena, B.K., Raj, C.R., 2006. Analytical Chemistry 78, 6332–6339.
Kang, S.M., Park, S., Kim, D., Park, S.Y., Ruoff, R.S., Lee, H., 2011. Advanced Functional Materials 21, 108–112.
Kuila, T., Bose, S., Khanra, P., Mishra, A.K., Kim, N.H., Lee, J.H., 2011. Biosensors and Bioelectronics 26, 4637–4648.
Lee, H., Dellatore, S.M., Miller, W.M., Messersmith, P.B., 2007. Science 318, 426–430.
Li, F.H., Yang, H.F., Shan, C.S., Zhang, Q.X., Han, D.X., Ivaska, A., Niu, L., 2009. Journal of Materials Chemistry 19, 4022–4025.
Liu, H.Y., Xi, P.X., Xie, G.Q., Shi, Y.J., Hou, F.P., Huang, L., Chen, F.J., Zeng, Z.Z., Shao, C.W., Wang, J., 2012. Journal of Physical Chemistry C 116, 3334–3341.
Maleki, A., Nematollahi, D., Clausmeyer, J., Henig, J., Plumeré, N., Schuhmann, W., 2012. Electroanalysis 24, 1932–1936.
Novoselov, K.S., Geim, A.K., Morozov, S.V., Jiang, D., Zhang, Y., Dubonos, S.V., Grigorieva, I.V., Firsov, A.A., 2004. Science 306, 666–669.
Tang, L., Zeng, G.M., Shen, G.L., Zhang, Y., Li, Y.P., Fan, C.Z., Liu, C., Niu, C.G., 2009. Analytical and Bioanalytical Chemistry 393, 1677–1684.
Wu, L.N., Zhang, X.J., Ju, H.X., 2007. Analytical Chemistry 79, 453–458.
Yang, D.W., Liu, H.H., 2009. Biosensors and Bioelectronics 25, 733–738.
Yang, L.P., Yee, W.A., Phua, S.L., Kong, J.H., Ding, H., Cheah, J.W., Lu, X.H., 2012. RSC Advances 2, 2208–2210.
Zeng, T., Zhang, X.L., Niu, H.Y., Ma, Y.R., Li, W.H., Cai, Y.Q., 2012. Applied Catalysis B: Environmental 134–135, 26–33.